Evolving morphotropic phase boundary in lead-free $(Bi_{1/2}Na_{1/2})TiO_3-BaTiO_3$ piezoceramics

Wook Jo,[1,a)] John E. Daniels,[2] Jacob L. Jones,[3] Xiaoli Tan,[4] Pamela A. Thomas,[5] Dragan Damjanovic,[6] and Jürgen Rödel[1]
[1]*Institute of Materials Science, Technische Universität Darmstadt, Petersenstr. 23, Darmstadt 64287, Germany*
[2]*School of Materials Science and Engineering, University of New South Wales, New South Wales 2052, Australia*
[3]*Department of Materials Science and Engineering, University of Florida, Gainesville, Florida 32611, USA*
[4]*Department of Materials Science and Engineering, Iowa State University, Ames, Iowa 50011, USA*
[5]*Department of Physics, University of Warwick, Coventry CV4 7AL, United Kingdom*
[6]*Ceramics Laboratory, Swiss Federal Institute of Technology (EPFL), Lausanne CH-1015, Switzerland*

(Received 12 July 2010; accepted 23 November 2010; published online 7 January 2011)

The correlation between structure and electrical properties of lead-free $(1-x)(Bi_{1/2}Na_{1/2})TiO_3-xBaTiO_3$ (BNT-100*x*BT) polycrystalline piezoceramics was investigated systematically by *in situ* synchrotron diffraction technique, combined with electrical property characterization. It was found that the morphotropic phase boundary (MPB) between a rhombohedral and a tetragonal phase evolved into a morphotropic phase region with electric field. In the unpoled material, the MPB was positioned at the transition from space group *R*3*m* to *P*4*mm* (BNT-11BT) with optimized permittivity throughout a broad single-phase *R*3*m* composition regime. Upon poling, a range of compositions from BNT-6BT to BNT-11BT became two-phase mixture, and maximum piezoelectric coefficient was observed in BNT-7BT. It was shown that optimized electrical properties are related primarily to the capacity for domain texturing and not to phase coexistence. © *2011 American Institute of Physics*. [doi:10.1063/1.3530737]

I. INTRODUCTION

It is well known that phase instabilities are responsible for optimizing the piezoelectric and dielectric properties of ferroelectric materials, and have thus been of great interest to the ferroelectric community for more than half a century.[1,2] One can identify two types of phase transitions in composition-temperature phase diagrams. The first is a polymorphic phase transition (PPT) where for a fixed composition the phase transition is temperature induced. Examples are cubic-tetragonal-orthorhombic-rhombohedral phase transitions in $(K_{1-x}Na_x)NbO_3$ solid solution for a given x.[2] The second is a morphotropic phase boundary (MPB) (Ref. 3) where a phase transition is induced by compositional modification, as in the case for $PbZrO_3-PbTiO_3$ (PZT), the market dominating electro-mechanical material.[2] For obtaining enhanced properties, the use of an MPB is favored over the use of a PPT, as it provides temperature-insensitive properties that are attractive for various applications. This has led to a significant increase in the contemporary understanding of the nature of MPB's.[4–15] The present search for new lead-free piezoceramics is thus focused on solid solutions exhibiting an MPB. These efforts have contributed further to the contemporary understanding of the nature of MPB.[16–21]

The $(1-x)(Bi_{1/2}Na_{1/2})TiO_3-100xBaTiO_3$ (BNT-100*x*BT) system has been of great interest since the discovery of an MPB, where a rhombohedral and a tetragonal symmetry coexist, in the system in 1991.[22] The interest has arisen largely because the MPB was reported to separate the rhombohedral BNT and the tetragonal BT as in PZT, accompanied by a significant enhancement in the dielectric permittivity and electromechanical coupling factor k_{33} (Ref. 22) as well as piezoelectric properties.[23,24] Although the presence of an MPB is rather evident in the literature with a view to the electrical properties, the structural similarity with PZT is still controversial. For example, contrary to most structural studies reporting that there is a clear transition from rhombohedral to tetragonal at $x=0.06-0.07$,[23–27] recent diffraction studies[28,29] have not clearly resolved the structure around the reported MPB composition, because a slight noncubic distortion is hard to resolve through diffraction techniques. It was further shown that a distinct noncubic distortion develops out of an apparently cubic symmetry, when the materials are exposed to an electric field.[28,30,31]

Considering that proper understanding of the correlation between structure and electrical properties is crucial in developing new materials, we performed a systematic investigation on BNT-100*x*BT ceramics for a wide range of compositions $(0\leq x\leq 0.15)$. To have an insight into the inconsistent literature report on the structure of BNT-100*x*BT, we analyzed the bulk structure of the materials using *in situ* synchrotron diffraction as a function of electric field from an initial unpoled state. Direction-dependent phase evolution (with relation to the applied field vector) under electric field and uniaxial stress were performed. The obtained structural aspects were compared and discussed with field-dependent permittivity (ε_{33}) and field-dependent piezoelectric coefficient (d_{33}) measured also *in situ* parallel to the electric field direction. These results enable a compari-

a)Electronic mail: jo@ceramics.tu-darmstadt.de.

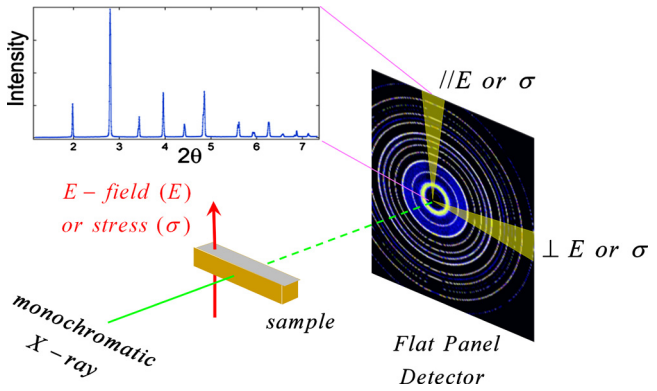

FIG. 1. (Color online) Schematic illustration of the setup for the *in situ* diffraction experiments.

son between the structural aspects near the MPB (e.g., phase identity, phase fraction, and domain texture) and the related properties.

II. EXPERIMENTAL PROCEDURE

Ceramic samples were prepared by a solid oxide route using reagent-grade powders. 24 h of planetary ball-milling were conducted before and after calcination at 900 °C for 3 h. Powder compacts were sintered at 1150 °C for 3 h. The details of the processing conditions can be found elsewhere.[32] Piezoelectric and dielectric properties were measured with disk-shaped samples by a commercial apparatus, aixPES (aixACCT Systems GmbH, Germany).

Bar-type bulk samples of dimensions $1\times1\times10$ mm^3 were used for *in situ* x-ray diffraction measurements at beamline ID15A/B of the European Synchrotron Radiation Facility.[30,33] Beam energies of 87.19 keV and 68.02 keV were selected for the *in situ* electric-field-dependent and stress-dependent experiments, respectively. At these beam energies, a 1 mm thick BNT-BT sample is transparent, and thus diffraction information is collected from the bulk of the material. The beam size was set prior to the sample to be 0.3×0.3 mm^2 by tungsten slits. Although the total fraction of grains in the gauge volume providing diffraction information may be small compared with the size of the specimen, this behavior can be extrapolated to all grains assuming a cylindrical symmetry around the field vector and from the fact that the average grain size is less than 2 μm. For electrical measurements, the sample was placed inside an *in situ* electric field chamber in order to apply electric fields perpendicular to the x-ray beam direction. Any possible electrical arcing or breakdown during the experiments that could lead to misinterpretation of the structural information was monitored by an additionally installed optical strain sensor. For stress measurements a Bose 3 kN load frame was used with a stress applied perpendicular to the x-ray beam direction. In both cases diffraction images were collected in the forward direction using Pixium 4700 flat panel detector as schematically shown in Fig. 1. In this geometry scattering vectors lie close to a plane perpendicular to the beam direction, and thus diffraction information can be isolated from grains with particular structural orientations to the applied field.

The two-dimensional diffraction images were segmented into 36 parts with a 10° interval azimuthally, and integrated using the software package FIT2D (Ref. 34) to obtain 36 one-dimensional diffraction patterns for specific orientations with a 10° increment. Among all the collected patterns, the patterns from the initial unpoled samples were used for Rietveld refinements, and the others for peak profile fitting. Rietveld refinement was performed using the software package Fullprof.[35] The wavelength and instrumental parameters were determined by refining a profile from a standard LaB_6 sample. During the refinements, the Bragg peaks were modeled by the Thompson–Cox–Hastings pseudo-Voigt function. The background was fit with selected points using a linear interpolation scheme. Zero angular shift, scale factor, lattice parameters, and atomic parameters were refined. The refinements were performed in a sequential manner from the structure of unmodified BNT, i.e., BNT-0BT,[36] with increasing barium concentration. The peak fitting module provided by the commercial software ORIGIN (Originlab, Inc., ver. 7.5) was used in order to extract peak intensities that are used in subsequent calculations of phase fraction and domain texture change. All the peaks were fit to the Voigt profile with the confidence band of 99%. As a semiquantitative indicator of the change in phase fractions, the intensity ratio between rhombohedral (200) and tetragonal (200) and (002) reflections is calculated using:

$$\mathrm{Rh}_{eff}=\frac{I_{200,r}}{I_{200,t}+I_{200,r}+I_{002,t}}, \tag{1}$$

where the subscript r and t denote rhombohedral and tetragonal, respectively.

In addition, both pseudocubic $(111)_{pc}$ (where the subscript "pc" represents the pseudocubic perovskite structure) and $(200)_{pc}$ reflections were fit to estimate the pole density of rhombohedral and tetragonal phases, respectively, using[37]

$$f_{111}(mrd)=4\frac{I_{111}/I^{U}_{111}}{I_{111}/I^{U}_{111}+3(I_{11\bar{1}}/I^{U}_{11\bar{1}})}, \tag{2}$$

and

$$f_{002}(mrd)=3\frac{I_{002}/I^{U}_{002}}{I_{002}/I^{U}_{002}+2(I_{200}/I^{U}_{200})}, \tag{3}$$

where I_{hkl} and I^{U}_{hkl} are the integrated intensities of diffraction peak hkl in the domain-oriented and unpoled (randomly oriented) sample, respectively. Here, I^{U}_{hkl} was obtained from a weighted average of the (002) and (200) Bragg reflections at 6 kV/mm for all orientations relative to the electric field following our previous work.[30] The parameters f_{002} and f_{111} describe the degree of 002 and 111 domain orientations in a particular direction of the sample and are described in more detail in Refs. 36 and 37. In the present case, the values reported are measured parallel to the electric field direction.

III. RESULTS AND DISCUSSION

Figures 2(a) and 2(b) display the $(200)_{pc}$ and $(210)_{pc}$ reflections from four representative diffraction patterns of unpoled samples in the composition range studied. BNT-0BT

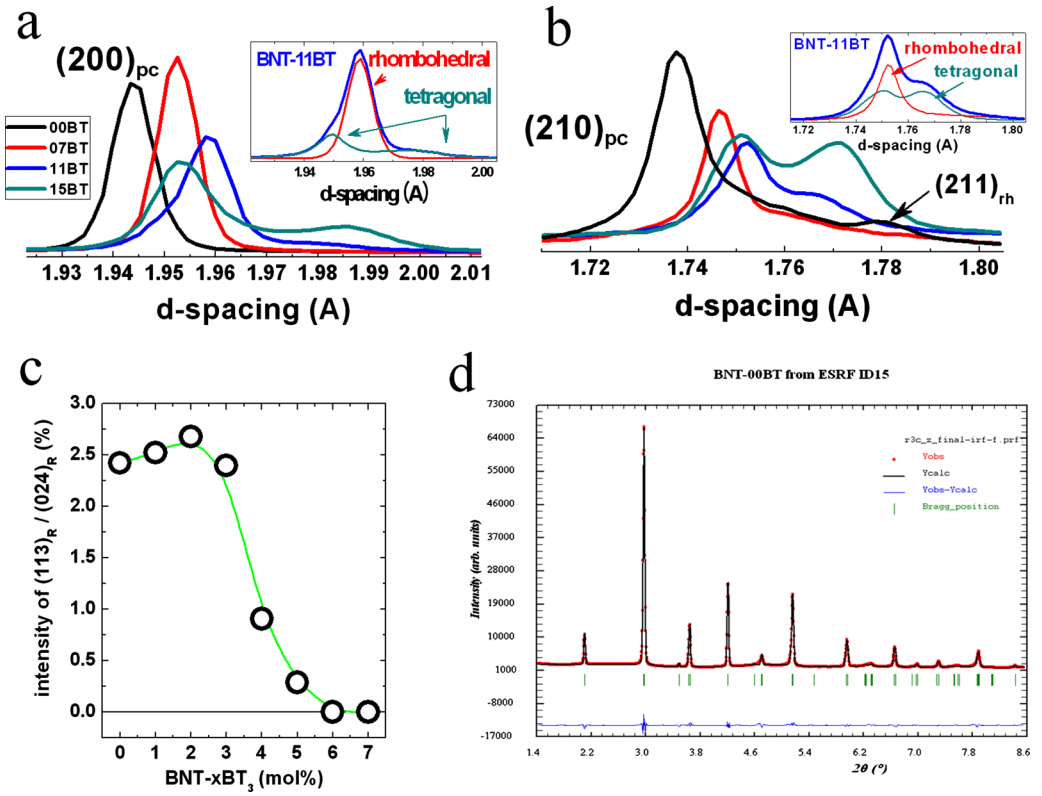

FIG. 2. (Color online) (a) and (b) show composition-dependent changes in pseudocubic (200) and (210) reflections, respectively. (c) Changes in the superlattice reflection 1/2(113) characteristic of oxygen octahedral tilting in rhombohedral symmetry. (d) An exemplary Rietveld fit used for the construction of the phase diagram presented in (a).

and BNT-15BT are clearly identified as rhombohedral $R3c$ with the presence of superlattice reflection[36] and tetragonal $P4mm$ with a clear splitting in the $(200)_{pc}$ reflection, respectively. On the other hand, BNT-7BT exhibits little trace of any noncubic distortion, which is consistent with the recent report.[29] As indicated in Fig. 2(c), the superlattice reflection featuring the $R3c$ space group[36] vanishes at $x \leq 0.06$. Rietveld refinement on the full-profiles from all the compositions investigated was performed prior to poling. Because the experimental setup used is not optimized for a precise determination of crystal symmetry but for efficient *in situ* experiments, a minimum number of parameters for the fit, such as the scale factor, zero angle shift, lattice parameters, backgrounds, and atomic parameters, were adjusted. Figure 2(d) provides a refinement for BNT-0BT as an example. The resulting Bragg R-factor (R_B), profile R-factor (R_P), and chi squared ($\chi 2$) were given 2.33, 2.59, and 4.18, respectively. For the compositions between BNT-6BT and BNT-10BT, various space groups such as $R3m$, $P4mm$, Cm, $Pm\bar{3}m$ were tested. The given refinement parameters favored either $R3m$ or $P4mm$ with a slight predominance over $R3m$. For example, resulting R_B, R_P, and $\chi 2$ for each structural model in the case of BNT-7BT were given respectively 1.37, 2.34, 3.61 for $R3m$, 1.40, 2.36, 3.83 for $P4mm$, 1.53, 2.35, 3.83 for Cm, and 2.10, 2.53, 4.20 for $Pm\bar{3}m$. However, from the fact that three distinctive reflections are denoted in the (200)pc reflection of BNT-11BT, the space group of the compositions between BNT-6BT and BNT10BT was assigned as $R3m$.

Figures 3(a) and 3(b) show the phase diagram of unpoled and poled (at 6 kV/mm) BNT-100xBT at room temperature, respectively. To trace the structural evolution due to the application of the electric field for the construction of Fig. 3(b), the characteristic reflections such as $(111)_{pc}$ for rhombohedral and $(200)_{pc}$ for tetragonal symmetry were deconvoluted. Changes in both phase content and properties due to the poling procedure are readily apparent. The structural transformation that might conventionally be regarded as one of the features of MPB occurs at BNT-11BT, which deviates significantly from the maximum in the electrical properties reported at $100x=6-7$ in the literature.[22–26] Dielectric properties of unpoled samples follow closely the presence of the $R3m$ symmetry, exhibiting a broad plateau with values between 1600 and 1800 in the composition space from BNT-5BT to BNT-11BT. Notice that a drastic change in relative permittivity, ε_r from BNT-11BT (ε_r about 1600) to BNT-12BT (ε_r about 1100) is coincident with the maximum in loss factor of 0.08, while in BNT-5BT a strong change only in ε_r is observed (with ε_r going from about 700 to 1700). In combination with the results from the structural analysis, one may assume that the anomaly observed for the BNT-5BT is a consequence of a slight change in the structure, i.e., a tilting-detilting transition, whereas that in BNT-11BT is indicative of much larger scale instability, e.g., a change in the point group symmetry.

There appears to be a clear discrepancy between positions of phase transition at BNT-5BT and at BNT-11BT and the broad maximum of electrical properties between 5 and 11 mol % BT for the unpoled material. Further, BNT-6BT

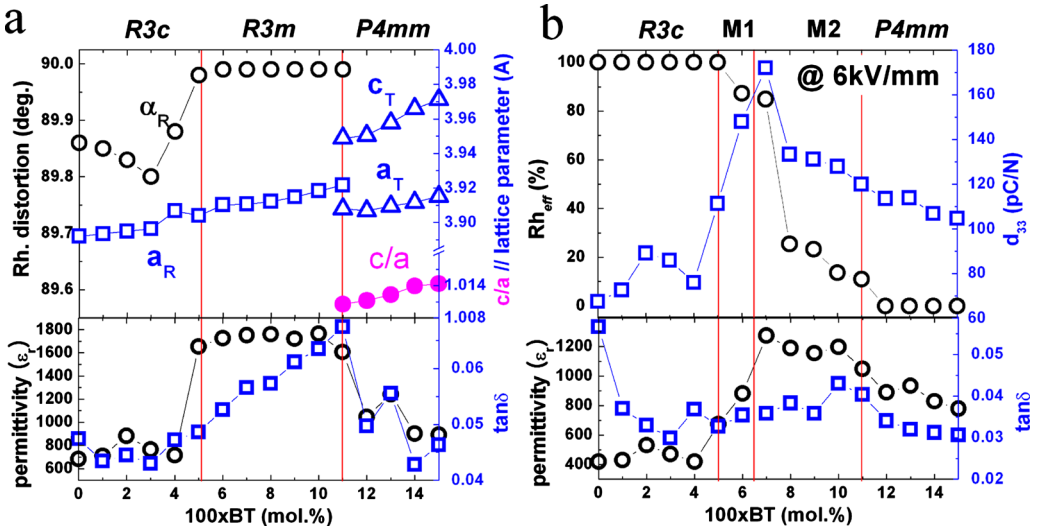

FIG. 3. (Color online) Phase diagram and dielectric properties (a) before and (b) after poling. Crystal structure and phase content of BNT-100xBT are contrasted to composition-dependent permittivity, loss factor (tan δ), and piezoelectric coefficient for (a) the unpoled material and (b) the poled material. Not only BNT-11BT that is initially at MPB but also the entire compositions having $R3m$ symmetry in their unpoled state evolve into a mixture of rhombohedral and tetragonal symmetries.

and BNT-7BT commonly referred to as the MPB compositions[16,22] where the permittivity is maximized coincide with none of the compositions of the structural instabilities identified in this study.

Consequently, we have conducted experiments to trace the structural evolution with electric field using an *in situ* synchrotron diffraction technique. Poling at 6 kV/mm at room temperature alters the phase fraction as provided in volume percent of rhombohedral phase [Rh_{eff} (percentage)] of BNT-100xBT drastically [Fig. 3(b)]. An extension in the composition range of two-phase coexistence is induced by the electric field, originally sharp at BNT-11BT to a broad region ranging from BNT-6BT to BNT-11BT. This is evidenced by the changes in the effective rhombohedral volume fraction determined from the intensity ratio of deconvoluted rhombohedral (200) over the total intensity of the pseudocubic $(200)_{pc}$ reflection. Four distinct structural regions are identified over the compositional range studied [Fig. 3(b)]. Both the space groups $R3c$ on the left hand side and the $P4mm$ on the right hand side of the compositional spectrum remain unaffected. However, initially $R3m$ rhombohedral compositions evolve into a two-phase mixture, either $R3c$ and $P4m(b)m$ (region M1) or $R3m$ and $P4mm$ (region M2). Note that the field-induced $P4mm$ phase could be $P4bm$ in M1 but no superlattice reflection indicating oxygen octahedral tilting can be detected. As expected, the compositional dependence of the dielectric properties changes significantly after the poling treatment. A sharp maximum in ε_{33} of about 1300 now appears at BNT-7BT. The piezoelectric coefficient exhibits a distinct maximum of 170 pC/N at BNT-7BT with BNT-6BT having a d_{33} of 150 pC/N and all other compositions with values of less than 140 pC/N.

This implies that the structural phase boundary that occurs at BNT-11BT is not responsible for the maximization of the electromechanical properties. Instead, this property enhancement is induced on the rhombohedral-rich side of the electric-field-induced MPB regime, i.e., at BNT-6BT and BNT-7BT.

Next, we discuss the phase evolution as observed by *in situ* synchrotron diffraction as a function of increasing, then decreasing electric field or uniaxial stress, as shown in Fig. 4. BNT-9BT is used as an example for the compositions with initially $R3m$ space group and mixed phase composition after poling. Figures 4(a) and 4(b) display the phase evolution as a function of electric field in the pseudocubic (200) peak with scattering vectors aligned parallel and perpendicular to the applied electric field, respectively. To promote an easier understanding of the contour plots shown, a surface plot corresponding to Fig. 4(a) is presented as an example in Fig. 5. It is seen that two additional reflections that refer to tetragonal (200) and (002) appear abruptly at a certain field level ($\sim$2 kV/mm) close to the initially existing rhombohedral (200) peak. Note that the electric-field-induced transition from the initial rhombohedral phase into a mixture of rhombohedral and tetragonal phases takes place concurrently in grains with [001] directions both parallel and perpendicular to the electric field vector. A direct comparison between Figs. 4(a) and 4(b) indicates clearly that the transition field is a very weak function of the direction of the applied electric fields. We also confirm that the same behavior is seen regardless of the sampled grain orientation angle to the applied electric field. These findings are consistent with those previously reported during *in situ* electrical loading.[28,30] In contrast, as shown in Fig. 4(c) (reflections with the scattering vector aligned parallel to the applied stress) and Fig. 4(d) (reflections with the scattering vector perpendicular to the stress), compressive stress induces the rhombohedral-to-tetragonal transition only along the direction perpendicular to the applied stress. The proposed mechanism for this phase transition is schematically illustrated in Fig. 6.

Following from the above, it appears that an additional factor other than phase coexistence plays an important role in maximizing properties. To investigate this, we monitored the evolution of piezoelectric coefficient d_{33} and permittivity ε_r of two compositions (BNT-7BT and BNT-9BT) *in situ* during the poling cycle [Figs. 7(a) and 7(b)]. Both materials are

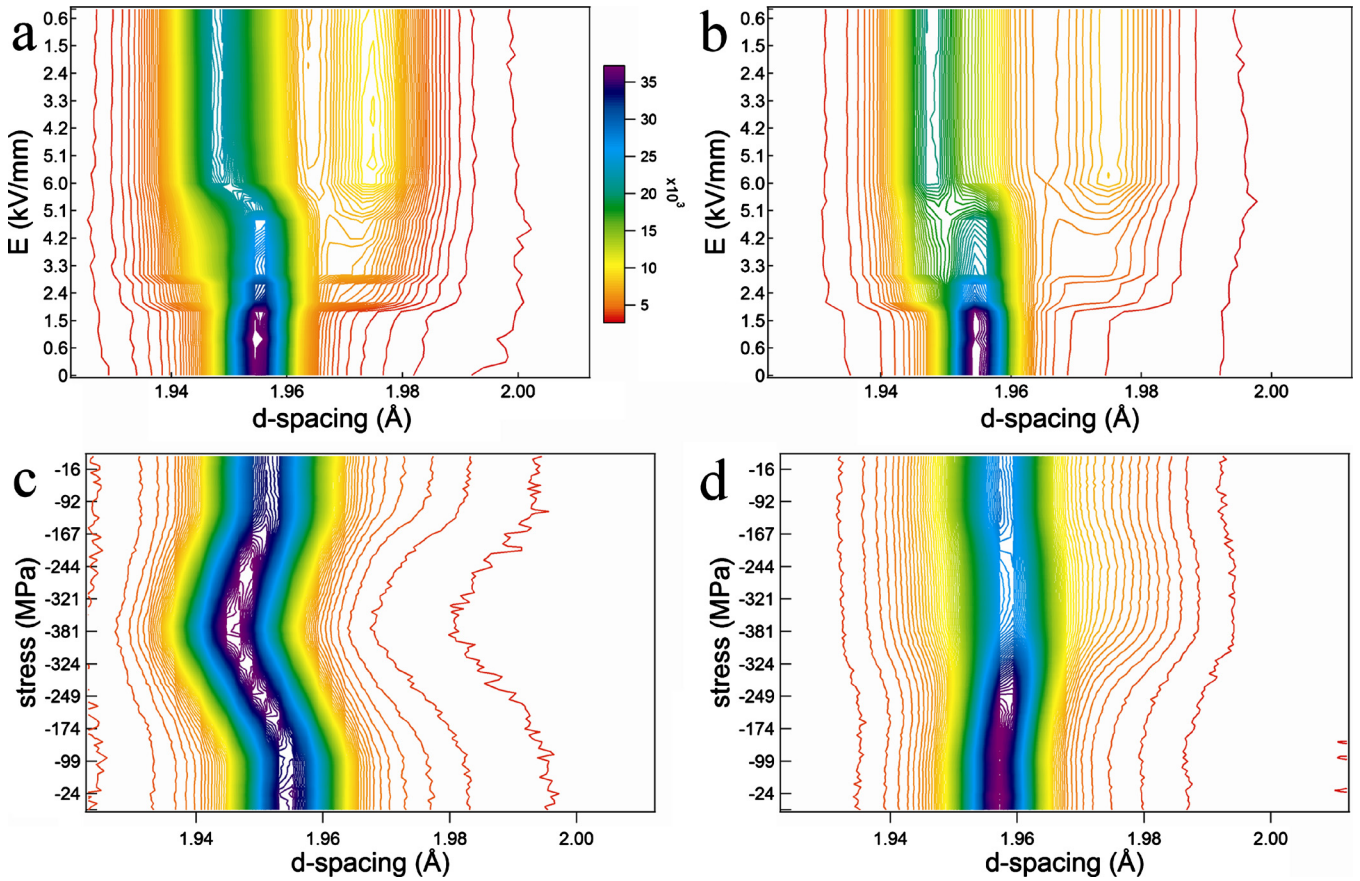

FIG. 4. (Color online) A contour plot with the scattering vector aligned (a) parallel and (b) perpendicular to the electric field as well as (c) parallel and (d) perpendicular to the mechanical load for BNT-9BT as a function of electric field. (a) and (b) show the electric field induced transformation occurring simultaneously in multiple grain orientations with applied electric field, while (c), and (d) show an orientation dependence of the phase transformation under applied stress field.

mixed phase (electrically-induced MPB) but one (BNT-7BT) exhibits enhanced properties and the other (BNT-9BT) does not. Note that once the rhombohedral-to-tetragonal phase transition is initiated, at 3 kV/mm in BNT-7BT and at 2 kV/mm in BNT-9BT, properties nearly saturate. At higher electric fields, especially in the case of BNT-9BT, the phase fraction of the rhombohedral phase (Rh_{eff}) changes from 90% to 30%, while d_{33} and ε_r change little. This suggests that phase fraction alone is not the dominant factor in enhancing properties.

All the experimental results so far suggest that the poling-induced electromechanical properties of the BNT-100xBT system could arise from another origin such as domain texture in the initially-existing rhombohedral phase. To quantify the contribution of domain reorientation to the piezoelectric properties, the pole density[38] for each phase was determined at 6 kV/mm along the poling direction [Fig. 7(c)]. The calculated pole density values for the tetragonal (f_{002}) and rhombohedral (f_{111}) phases provide an insight into why all MPB compositions (in the structural sense) do not exhibit optimum electrical properties. Domain switching is notably absent in the electric-field-induced tetragonal phase in all the MPB compositions except for BNT-6BT and BNT-7BT. This implies that 90° domain switching in the tetragonal phase is absent[39] in all the compositions between BNT-8BT and BNT-11BT. In contrast, the BNT-7BT material

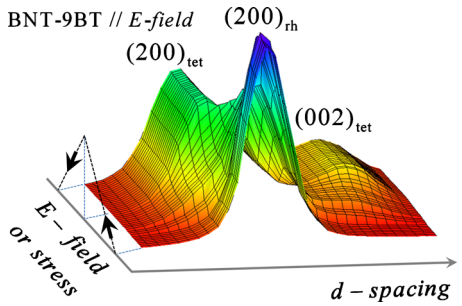

FIG. 5. (Color online) The corresponding surface plot for the contour plot presented in Fig. 4(a). This is intended to provide a reference with which one can comprehend the contour plots presented in Figs. 4(a)–4(d) easier.

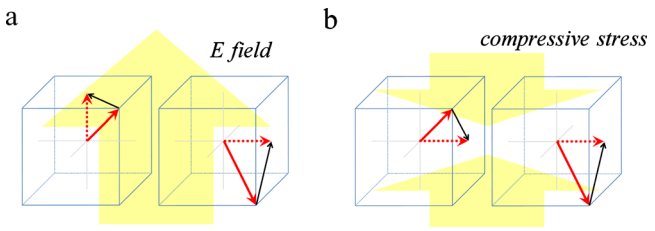

FIG. 6. (Color online) Schematic illustrations showing how a, electric field and b, compressive stress induce the tetragonal symmetry out of the rhombohedral. Red and black arrows denote polarization vector and path through which polarization can rotate, respectively (Ref. 5).

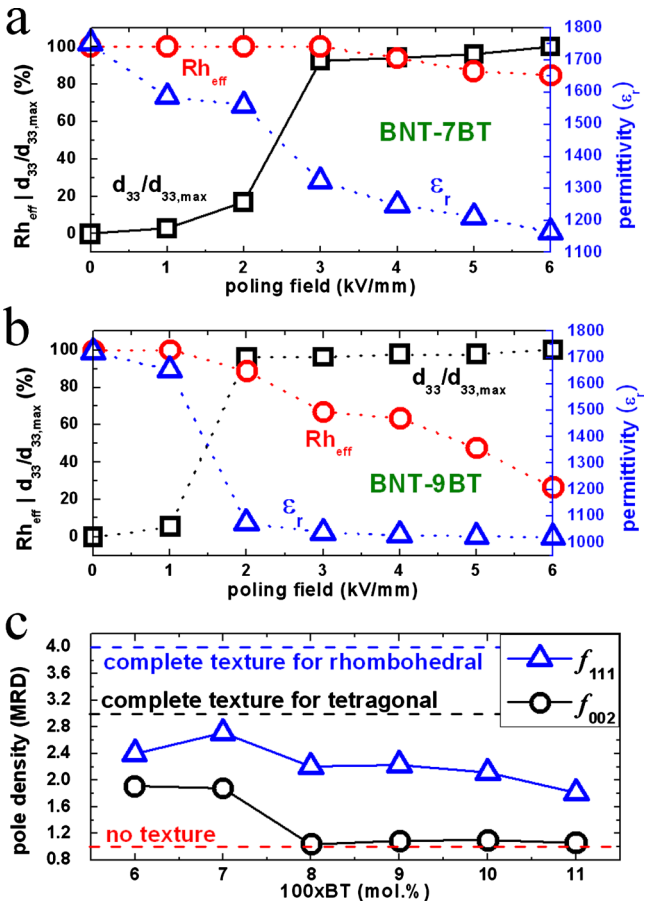

FIG. 7. (Color online) Evolution of piezoelectric coefficient (d_{33}), relative permittivity (ε_r), and an effective rhombohedral volume fraction (Rh_{eff}) of (a) BNT-7BT and (b) BNT-9BT during poling. (c) Calculated pole densities that represent the degree of domain reorientation during poling of each composition (up to 6 kV/mm). In the case of BNT-6BT and BNT-7BT, not only the rhombohedral but also the induced tetragonal phases develop a high degree of texture, while practically no texture develops in the induced tetragonal phases in other compositions. The size of the symbols is slightly larger than the error range in Rh_{eff} and pole densities. The dotted lines in (a) and (b) *trace the evolution of* ε_r and d_{33} during loading and unloading of electric fields.

shows a maximum degree of domain texture both in the tetragonal and rhombohedral phases, which correlates with the observed maximized electrical properties. Hence, both the presence of a phase coexistence region and the ability to induce optimum domain texture determine the composition where optimum electrical properties are obtained.

IV. SUMMARY AND CONCLUSIONS

In summary, salient results revolve around the position of an either sharp or broad MPB (or regime) before and after poling and its relation to electrical properties. Also, next to phase composition, texture is highly pertinent. These issues can be focused onto three central points:

- Phase composition in BNT-100xBT changes from the unpoled to the poled material in the regime of the MPB.
- Specifically, the position of the most drastic structural change (MPB) and the composition with best electrical properties evolve with electric field: In the unpoled material, a broad maximum is obtained in the single-phase $R3m$ compositions (between BNT-5BT and BNT-11BT), while in the poled material, a clear maximum in piezoelectric coefficient occurs at BNT-7BT.
- Phase coexistence alone is not sufficient to provide optimum electrical properties but has to be combined with optimum ability for domain reorientation, or domain texture evolution.

ACKNOWLEDGMENTS

W.J. thanks T. Granzow, K. G. Webber, S. Schaab, and J. Glaum for discussions as well as J.-B. Ollagnier, E. Aulbach, M. Hinterstein, M. Ehmke, and M. Heyse for experimental assistance. Authors thank I. Reaney and K. Albe for critical review. The work by W.J. and J.R. was sponsored through the state center ADRIA. The European Synchrotron Radiation Facility is acknowledged for the provision of experimental time. J.D. acknowledged financial support through an AINSE research fellowship. J.J. acknowledges support from the U.S. Department of the Army under Grant No. W911NF-09-1-0435 and the U.S. National Science Foundation (NSF) under Award No. DMR-0746902.

[1]G. H. Haertling, J. Am. Ceram. Soc. **82**, 797 (1999).
[2]B. Jaffe, W. R. Cook, and H. Jaffe, *Piezoelectric Ceramics* (Academic, London, 1971), Vol. 3.
[3]Although, in principle, any phase boundary where a structural change occurs with compositional modification may be labeled an MPB, the term MPB is confined to the context where structural change leads to an increase in the multiplicity of polarization states, and therefore potentially contributes to an enhancement of electromechanical properties.
[4]S.-E. Park and T. R. Shrout, J. Appl. Phys. **82**, 1804 (1997).
[5]H. Fu and R. E. Cohen, Nature (London) **403**, 281 (2000).
[6]R. Guo, L. E. Cross, S.-E. Park, B. Noheda, D. E. Cox, and G. Shirane, Phys. Rev. Lett. **84**, 5423 (2000).
[7]B. Noheda, D. E. Cox, G. Shirane, S.-E. Park, L. E. Cross, and Z. Zhong, Phys. Rev. Lett. **86**, 3891 (2001).
[8]M. Ahart, M. Somayazulu, R. E. Cohen, P. Ganesh, P. Dera, H.-K. Mao, R. J. Hemley, Y. Ren, P. Liermann, and Z. Wu, Nature (London) **451**, 545 (2008).
[9]A. Bell, J. Mater. Sci. **41**, 13 (2006).
[10]G. A. Rossetti, A. G. Khachaturyan, G. Akcay, and Y. Ni, J. Appl. Phys. **103**, 114113 (2008).
[11]Y. Ishibashi and M. Iwata, Jpn. J. Appl. Phys., Part 2 **37**, L985 (1998).
[12]R. Theissmann, L. A. Schmitt, J. Kling, R. Schierholz, K. A. Schönau, H. Fuess, M. Knapp, H. Kungl, and M. J. Hoffmann, J. Appl. Phys. **102**, 024111 (2007).
[13]W. Cao and L. E. Cross, Phys. Rev. B **47**, 4825 (1993).
[14]Z. Kutnjak, J. Petzelt, and R. Blinc, Nature (London) **441**, 956 (2006).
[15]T. Leist, W. Jo, T. Comyn, A. Bell, and J. Rödel, Jpn. J. Appl. Phys. **48**, 120205 (2009).
[16]J. Rödel, W. Jo, K. T. P. Seifert, E. M. Anton, T. Granzow, and D. Damjanovic, J. Am. Ceram. Soc. **92**, 1153 (2009).
[17]Y. Saito, H. Takao, T. Tani, T. Nonoyama, K. Takatori, T. Homma, T. Nagaya, and M. Nakamura, Nature (London) **432**, 84 (2004).
[18]T. R. Shrout and S. J. Zhang, J. Electroceram. **19**, 113 (2007).
[19]R. J. Zeches, M. D. Rossell, J. X. Zhang, A. J. Hatt, Q. He, C.-H. Yang, A. Kumar, C. H. Wang, A. Melville, C. Adamo, G. Sheng, Y.-H. Chu, J. F. Ihlefeld, R. Emi, C. Ederer, V. Gopalan, L. Q. Chen, D. G. Schlom, N. A. Spaldin, L. W. Martin, and R. Ramesh, Science **326**, 977 (2009).
[20]T. Takenaka, H. Nagata, and Y. Hiruma, Jpn. J. Appl. Phys. **47**, 3787 (2008).
[21]P. K. Panda, J. Mater. Sci. **44**, 5049 (2009).
[22]T. Takenaka, K.-I. Maruyama, and K. Sakata, Jpn. J. Appl. Phys., Part 1 **30**, 2236 (1991).
[23]M. Chen, Q. Xu, B. H. Kim, B. K. Ahn, J. H. Ko, W. J. Kang, and O. J. Nam, J. Eur. Ceram. Soc. **28**, 843 (2008).

[24]B.-J. Chu, D.-R. Chen, G.-R. Li, and Q.-R. Yin, J. Eur. Ceram. Soc. **22**, 2115 (2002).
[25]D. Rout, K. S. Moon, V. S. Rao, and S.-J. L. Kang, J. Ceram. Soc. Jpn. **117**, 797 (2009).
[26]Y. S. Sung, J. M. Kim, J. H. Cho, T. K. Song, M. H. Kim, and T. G. Park, Appl. Phys. Lett. **96**, 202901 (2010).
[27]B. Wylie-van Eerd, D. Damjanovic, N. Klein, N. Setter, and J. Trodahl, Phys. Rev. B **82**, 104112 (2010).
[28]J. E. Daniels, W. Jo, J. Rödel, and J. L. Jones, Appl. Phys. Lett. **95**, 032904 (2009).
[29]R. Ranjan and A. Dviwedi, Solid State Commun. **135**, 394 (2005).
[30]J. E. Daniels, W. Jo, J. Rödel, V. Honkimäki, and J. L. Jones, Acta Mater. **58**, 2103 (2010).
[31]Q. Zhang, Y. Zhang, F. Wang, Y. U. Wang, D. Lin, X. Zhao, H. Luo, W. Ge, and D. Viehland, Appl. Phys. Lett. **95**, 102904 (2009).
[32]W. Jo, T. Granzow, E. Aulbach, J. Rödel, and D. Damjanovic, J. Appl. Phys. **105**, 094102 (2009).
[33]K. G. Webber, Y. Zhang, W. Jo, J. E. Daniels, and J. Rödel, J. Appl. Phys. **108**, 014101 (2010).
[34]A. P. Hammersley, S. O. Svensson, M. Hanfland, A. N. Fitch, and D. Hausermann, High Press. Res. **14**, 235 (1996).
[35]T. Roisnel and J. Rodriguez-Carvajal, Mater. Sci. Forum **378**, 118 (2001).
[36]G. O. Jones and P. A. Thomas, Acta Crystallogr., Sect. B: Struct. Sci. **58**, 168 (2002).
[37]A. Pramanick, J. E. Daniels, and J. L. Jones, J. Am. Ceram. Soc. **92**, 2300 (2009).
[38]J. L. Jones, B. J. Iverson, and K. J. Bowman, J. Am. Ceram. Soc. **90**, 2297 (2007).
[39]J. Y. Li, R. C. Rogan, E. Üstündag, and K. Bhattacharya, Nature Mater. **4**, 776 (2005).